ELSEVIER

Biophysical Chemistry 90 (2001) 57–74

Biophysical Chemistry

www.elsevier.nl/locate/bpc

Interaction of Zn^{2+} with phospholipid membranes

H. Binder[a,*], K. Arnold[a], A.S. Ulrich[b], O. Zschörnig[a]

[a] *University of Leipzig, Institute of Medical Physics and Biophysics, Liebigstr. 27, D-04103 Leipzig, Germany*
[b] *Friedrich-Schiller-University of Jena, Institute of Molecular Biology, Winzerlaer Str. 10, 07745 Jena, Germany*

Received 19 July 2000; received in revised form 18 December 2000; accepted 18 December 2000

Abstract

To characterize the specificity of zinc binding to phospholipid membranes in terms of headgroup structure, hydration and phase behavior we studied the zwitterionic lipid 1-palmitoyl-2-oleoyl-phosphatidylcholine as a function of hydration at 30°C in the presence and absence of $ZnCl_2$. Zinc forms a 2:1–1:1 complex with the lipid, and in particular with the negatively charged phosphate groups. Zn^{2+}-bridges between neighboring lipid molecules stabilize the gel phase of the lipid relative to the liquid–crystalline state. Upon Zn^{2+} binding the C–O–P–O–C– backbone of the lipid headgroup changes from a *gauche/gauche* into the *trans/trans* conformation and it loses roughly 50% of the hydration shell. The ability of the Zn^{2+}-bound phosphate groups to take up water is distinctly reduced, meaning that the headgroups have become less hydrophilic. The energetic cost (on the scale of Gibbs free energy) for completely dehydrating the lipid headgroups is decreased by approximately 10 kJ/mole in the presence of Zn^{2+}. The interaction of phospholipid headgroups with Zn^{2+} is conveniently described by a hydrated zinc–phosphate complex the key energy contribution of which is more covalent than electrostatic in nature. Dehydration of phospholipid headgroups due to complexation with zinc cations is suggested to increase fusogenic potency of lipid membranes. Zinc appears to be one of the most potent divalent cation in inducing membrane fusion. © 2001 Elsevier Science B.V. All rights reserved.

Keywords: Lipid hydration; Divalent cations; Membrane fusion; IR linear dichroism

1. Introduction

Among the first-row transition metals, zinc is second only to iron in terms of abundance and importance in chemical, structural and regulatory roles in biological systems (see [1] and references cited therein). The coordination chemistry of zinc is as versatile as the metal ion function in biology, and this function is governed to a great degree by the metal ligands. It easily accommodates nitrogen, oxygen and sulfur atoms. Zinc binds to negatively charged residues (e.g. carboxylates and thiolates) via coulombic charge–charge interactions and to neutral residues (e.g. carbonyls and imidazoles) via orientation-dependent charge–dipolar interactions as well [2,3]. In addition, molecular orbital effects make an important contribution to the energetics and coordination of zinc complexes

* Corresponding author. Tel.: +49-341-9732476; fax: +49-341-9715709.
E-mail address: binder@rz.uni-leipzig.de (H. Binder).

0301-4622/01/$ - see front matter © 2001 Elsevier Science B.V. All rights reserved.
PII: S0301-4622(01)00130-2

accounting for the favorable binding of zinc to tetrahedral sites. The biological function of zinc is at least partially governed by the composition of its tetrahedral coordination polyhedron in metalloproteins. Also water potentially participates as a ligand in zinc coordination polyhedra.

Although zinc is essential for catalytic activity of several enzymes such as peptidases [4], phospholipases [5,6] and channel-forming Alzheimer's disease amyloid beta-protein [7] the role of Zn^{2+} is in many cases more structural than catalytic. The interaction of Zn^{2+} with nucleic acids can significantly influence their structure and function (see [8] and references cited therein). The binding of zinc to nucleobases can destabilize DNA and cause local denaturation of double helix on the one hand. On the other hand, some three-dimensional DNA architectures such as intramolecular triplexes, kinks and hairpins were stabilized in the presence of Zn^{2+}. This cation also influences the formation of protein–DNA complexes where it is required for DNA-binding activity because the metal ions probably stabilizes the nucleic acid-binding domain of proteins in order to maintain the proper topology for nucleic acid association.

In our preceeding paper we studied complex formation of zinc with 'B18', the histidine-rich motif HxxHH of a short polypeptide sequence of 18 residues [9]. Binding of zinc to B18 has been shown to stabilize an α-helical secondary structure in aqueous solution [9,10] and at semidry conditions [9]. B18 represents the minimal membrane-binding and fusogenic motif of the sea urchin sperm protein 'bindin' which plays a key role in fertilization, as it mediates the species-specific gamete adhesion and presumably fusion with the egg membrane [11,12]. The polypeptide B18 causes rapid and effective fusion between uncharged lipid vesicles only in the presence of Zn^{2+} [10]. In this case zinc seems to act as a folding-aid by introducing a local peptide conformation resembling the native zinc-binding site of the parent protein. This hypothesis neglects specific interactions of the metal cations with lipid membranes that potentially can interfere with the effect of zinc on peptide conformation.

It is known that zinc ions are capable of inducing fusion of phospholipid vesicles on its own at concentrations considerably lower than were required for other divalent cations such as Ca^{2+} [13]. Moreover, Ca^{2+} and Zn^{2+} possess synergistic effects on membrane fusion [14]. Because the reported fusogenic effect of zinc is far more extensive than effects with other cations this species appears to be relatively potent in inducing membrane fusion. This property and the high amounts of Zn^{2+} that are located in brain tissue suggest involvement of zinc into synaptic transmission, and in particular into fusion of intracellular vesicles containing neurotransmitter with the cytoplasmatic nerve membrane [15].

In general, metal ions bind to membranes in two steps [16]. At first, long range electrostatic interactions can strongly increase the local concentration of ions near the membrane surface. For example, lipids with anionic headgroups such as phosphoserine or phosphoglycerol attract cations to a considerable degree [17]. In a second step metal ions penetrate into the polar region of the membrane and form complexes with specific sites. The mode of metal ion binding preferentially involves the phosphodiester and carbonyl groups and the water of the hydration shell of the lipids and ions as well [17].

Here we focus our attention on the second step of ion binding to characterize the specificity of zinc-phospholipid interactions. To this aim, we studied bilayers of a neutral zwitterionic lipid as a function of water activity in the presence and absence of zinc. This approach is expected to yield information about intermolecular interactions in the polar region of the membranes including zinc and water. The general process of membrane fusion must involve a sequence of events, namely vesicle aggregation, surface dehydration and membrane destabilization, before the final merging of the bilayers can proceed. Hydration of polar interfaces and the repulsive forces acting between them are obviously closely related to the ability of lipid bilayers to fuse [18]. Consequently, an investigation of the membrane system as a function of hydration is expected to yield information about their fusogenic potency. Recently, we combined hydration/dehydration studies with infrared (IR) linear dichroism measurements to characterize the molecular architecture

of lipid systems [19–21]. Here this spectroscopic technique is applied to deal with the current problem.

The paper is organized as follows: First, we examine the binding of Zn^{2+} to the phosphatidylcholine (PC) headgroups, their conformational response and the stoichiometry of the Zn^{2+}/lipid complex. Second, we compare the water adsorption and the lyotropic chain melting transition of the lipid in the presence and absence of Zn^{2+}.

2. Materials and methods

2.1. Materials and preparation of lipid vesicles

Vesicles of 1-palmitoyl-2-oleoyl-*sn*-glycero-3-phosphocholine (POPC, Avanti Polar Lipids, Alabaster, USA) were prepared as follows. The lipid in a chloroform/methanol stock solution (1:3 v/v), was dried and re-suspended by vortexing in water (D_2O or H_2O) at final lipid concentration of 2–3 mg/ml, followed by extrusion (Lipex extruder, Biomembranes, Vancouver, Canada) of the suspension through a polycarbonate Unipore membrane (100 nm pore-size, Millipore).

Sample solutions were prepared by mixing appropriate amounts of stock solutions of the lipid and of $ZnCl_2$ (dissolved in D_2O or H_2O, 10 mM) to yield nominal Zn^{2+}-to-lipid ratios between $R_{Z/L} = 0$ and 3 (mol/mol). Before measurements the sample solutions were stored overnight at $T \approx 4$°C.

2.2. IR linear dichroism measurements

Samples were prepared by pipetting 100–200 μl of the sample solution on a ZnSe attenuated total reflection (ATR) crystal ($70 \times 10 \times 5$ mm^3 trapezoid, face angle 45°, six active reflections) and evaporating the water under a stream of warm air. While drying, the material was spread uniformly over an area of $A_{\text{film}} \approx 40 \times 7$ mm^2 onto the crystal surface by gently stroking with the pipette tip. The amount of material corresponds to an average thickness of the dry film of $d_0 > 3$ μm, assuming a density of 1 g/cm^3.

The ATR crystal was mounted into a commercial horizontal ATR holder (Graseby Specac, Kent, UK) that had been modified such as to realize a well-defined relative humidity (RH) and temperature (T) within the sample chamber [19]. We used a flowing water thermostat (Julabo, Seelbach, Germany) and a moisture generator (HumiVar, Leipzig, Germany) to adjust RH (D_2O or H_2O) to any value between 5 and 95%, with an accuracy of $\pm 0.5\%$ at $T = 30$°C. Polarized absorbance spectra, $A_{\parallel}(\nu)$ and $A_{\perp}(\nu)$ (128 scans, nominal resolution 2 cm^{-1}), were recorded by means of a BioRad FTS-60a Fourier transform infrared spectrometer (Digilab, MA, USA) at two perpendicular polarizations of the IR beam, parallel ($\parallel$) and perpendicular ($\perp$) with respect to the plane of incidence.

Before starting the measurements, the lipid films were hydrated for one hour at RH = 95% and subsequently dried at 5%. Then, RH was increased stepwisely (hydration scan). Polarized spectra were recorded every 3% after allowing the sample to equilibrate for 10 min at each step. After reaching the maximum value of RH, the scan direction was reversed (dehydration scan). In the samples without $ZnCl_2$, no hysteresis effects were detected. In the presence of $ZnCl_2$ the formation of a complex between POPC and Zn^{2+} (vide infra) was observed in the first hydration scan only after reaching a humidity of RH > 60%. Hence, this structure obviously requires an equilibration period of several hours in an atmosphere of moderate to high humidity. At molar ratios of $ZnCl_2$/POPC, $R_{Z/L} < 1$, the complex remains stable after subsequently drying the film. At $R_{Z/L} \geq 1$, however, it partially decomposes at a humidity below 40%. The complex forms again at RH > 60% in these samples. In view of this hysteresis, we exclusively present the results of dehydration scans.

Although we used D_2O vapor in most measurements, some experiments were performed with H_2O to prove that the spectrum of adsorbed D_2O, and in particular its bending mode near (1200–1204) cm^{-1}, does not lead to a misinterpretation of the IR spectra, especially of the narrow $\nu_{as}(PO_2^-)_{Zn}$ mode which also occurs at 1204 cm^{-1} (vide infra).

2.3. Spectral analysis in terms of IR order parameter and sample composition

The IR order parameter, S_{IR}, of an absorption band was calculated by means of

$$S_{IR} = \frac{R - K_1^{\infty}}{R + K_2^{\infty}} \quad \text{with} \quad R \equiv \frac{A_{||}}{A_{\perp}} \tag{1}$$

The polarized absorbances, $A_{||}$ and $A_{\perp}$, were evaluated from $A_{||}(\nu)$ and $A_{\perp}(\nu)$ by integration after baseline correction. In some cases the bands were separated using a global fitting technique [22]. In general, the 'constants' $K_1(\xi) \equiv (E_{z'}/E_{y'})^2 + (E_{x'}/E_{y'})^2$ and $K_2(\xi) \equiv (E_{z'}/E_{y'})^2 - (E_{x'}/E_{y'})^2$ depend on the Cartesian coordinates of the normalized electric field amplitude (z' and y' point normal to the ATR surface and to the plane of incidence, respectively). These components depend on the ratio of the thickness of the sample film over the wavelength of the light ($\xi \equiv d/\lambda$), on the angle of incidence ($\omega = 45°$), and on the ratio of the refractive indices of the sample and the ATR crystal ($n_{21} = n_{sample}/n_{ZnSe} = 0.58$) [23]. We make use of the 'thick' film approximation ($K_1^{\infty} = 2$ and $K_2^{\infty} = 2.54$, [23]) which has been shown to yield acceptable results for lipid films on a ZnSe crystal at $\xi \geq 0.2$ [22].

The peak position and the center of gravity, $COG \equiv \int \nu A(\nu) d\nu / \int A(\nu) d\nu$ of an absorption band were determined from the weighted and baseline corrected sum spectrum $A(\nu) = A_{||}(\nu) + K_2^{\infty} A_{\perp}(\nu)$ [21,22].

Let us consider two absorbing states of a moiety, A and B, which can be distinguished by two separate, closely spaced absorption bands, $\varepsilon_i \cdot G_i(\nu)$ (i = A, B). Here $G_i(\nu)$ denotes the normalized shape of each band (area = 1) and ε_i is the integral molar absorption coefficient. The spectral range of interest represents the superposition of both modes, $A(\nu) = x_A \cdot \varepsilon_A G_A(\nu) + (1 - x_A) \cdot \varepsilon_B G_B(\nu)$, in the absence of parasite bands. One obtains the following equation for the mole fraction of the moiety in state A after calculating the center of gravity (vide supra) and rearrangement

$$x_A = \frac{(COG - COG_B)}{(g \cdot COG_A - COG_B) - COG \cdot (g - 1)} \quad \text{with} \quad g \equiv \frac{\varepsilon_A}{\varepsilon_B} \tag{2}$$

COG_A and COG_B are the center of gravity of the absorption bands of the pure species which correspond to $x_A = 1$ and 0, respectively.

2.4. Determination of water adsorption isotherms by means of ATR-IR spectroscopy

The integral absorbance of a vibrational mode depends on the number of active internal reflections (N_{ref}), the concentration of the absorbing molecules within the film (c), the number of absorbing groups per molecule (n), their integrated molar absorption coefficient (ε), and the so-called penetration depth of electromagnetic waves into the sample film ($d_p = \lambda \cdot a^{-1}$; $a = 2\pi(\sin^2\omega \cdot n_{ZnSe}^2 - n_{sample}^2) \approx 6$ [23]) [22]:

$$A \equiv A_{||} + K_2 A_{\perp} = L_{iso} d_p \cdot N_{ref} c n \varepsilon \tag{3}$$

The function

$$L_{iso}(\xi) = \frac{n_{21}}{2\cos\omega} \cdot (1 - \exp(-2a\xi)) \cdot \times (K_1(\xi) + K_2(\xi)) \tag{4}$$

considers the effective optical pathlength of the corresponding isotropic sample per internal reflection. For a water/lipid mixture the concentrations of the components are $c_W = N_W/(v_L N_L + v_W N_W) = R_{W/L}(v_L \phi)^{-1}$ and $c_L = N_L/(v_L N_L + v_W N_W) = (v_L \phi)^{-1}$ (molar volumes $v_W \approx 0.018$ l/mole and $v_L \approx 0.78$ l/mol). Hence, the integrated absorbance of a selected IR active mode of the water and of the lipid centered around λ_W and λ_L, respectively, represent functions of the molar ratio water-to-lipid, $R_{W/L} = N_W/N_L$, of the swelling factor, $\phi = 1 + R_{W/L} v_W / v_L$, and of the relative thickness of the film, $\xi_i = d_0 \cdot \phi / \lambda_i (i = w, L)$:

$$A_W = \frac{N_{\mathrm{ref}} \cdot \lambda_W \cdot \varepsilon_W \cdot L_{\mathrm{iso}}(\xi_W)}{a \cdot v_L \cdot \phi} \cdot R_{W/L} \quad \text{and}$$

$$A_L = \frac{N_{\mathrm{ref}} \cdot \lambda_L \cdot n_L \cdot \varepsilon_L \cdot L_{\mathrm{iso}}(\xi_L)}{a \cdot v_L \cdot \phi} \tag{5}$$

Combination of these equations and rearrangement yields $R_{W/L}$ as a function of optical quantities:

$$R_{W/L} = \frac{\lambda_L \varepsilon_L n_L}{\lambda_W \varepsilon_W} \cdot \frac{L_{\mathrm{iso}}(\xi_L)}{L_{\mathrm{iso}}(\xi_W)} \cdot \frac{A_W}{A_L} \approx K \cdot \frac{A_W}{A_L} \tag{6}$$

In general, the position of the absorption band, its absorption coefficient and the film thickness are functions of $R_{W/L}$, because the physicochemical properties and the volume of the sample vary with progressive hydration. In practice, the wavenumber remains virtually constant at $\nu > 1500\ \mathrm{cm}^{-1}$ ($|\Delta\lambda|/\lambda < 0.03$) because the absorption frequencies of the dry and fully hydrated lipid typically differ by less than 50 cm^{-1} (vide infra). The thickness of the film is expected to swell by $1 < \phi < 1.3$ if each lipid adsorbs $0 < R_{W/L} < 12$ water molecules. The corresponding change of L_{iso} is small and similar for both absorption bands at $\xi > 0.2$ ($|\Delta L_{\mathrm{iso}}|/L_{\mathrm{iso}} < 0.05$) and therefore it can be neglected in Eq. (6).

In preliminary experiments we found that the integrated intensity of the C–H stretching region of POPC (3000–2800 cm^{-1}) decreases by (35% over the range of hydration considered here. Eq. (5) predicts for $\varepsilon \cdot L_{\mathrm{iso}} = \mathrm{const}$ that A_L weakens by $\sim 20\%$ in contrast to this result. The extinction of the intense methylene stretching bands is known to be sensitive to the state of the acyl chains [24]. Obviously the choice of an appropriate reference band represents the most critical factor to quantify water adsorption by means of Eq. (6). The $\nu(\mathrm{C=O})$ band provides a better internal standard, because its integrated intensity (1780–1690 cm^{-1}) decreases upon hydration by $\sim 25\%$ which is close to the expected value. The shape and position of the broad O–D (or O–H) stretching band of D_2O, $\nu_{13}(D_2O)$, (or $\nu_{13}(H_2O)$) changes only slightly with increasing RH (data not shown; for H_2O, see Pohle et al. [25]). Hence, it is justified to assume virtually constant values $\varepsilon_L((\mathrm{C=O}))$ and $\varepsilon_W(\nu_{13})$ under isothermal conditions. Then, $R_{W/L}$ can be estimated directly from the ratio of the integrated absorbances by means of $R_{W/L} \approx K \cdot A_W(\nu_{13})/A_L(\nu(\mathrm{C=O}))$. This approximation is confirmed by comparison with the POPC isotherms, which were measured both gravimetrically and by IR spectroscopy to yield the proportionality constant K (see below and Fig. 4). The $\nu_{13}(D_2O)$ band was integrated over the range 2700–2100 cm^{-1}, and $\nu_{13}(H_2O)$ over 3700–3100 cm^{-1}.

The adsorption of water to free $ZnCl_2$ is determined in POPC/$ZnCl_2$ mixtures at $x_Z > 0.5$ and $x_Z = 0.5$ (cf. Eqs. (B5) and (B6) in Appendix B)

$$R_{W/L}(Z) \equiv R_{W/Z}(Z) \cdot R_{Z/L} \approx K \times \left\{ \left(\frac{A_W(\nu_{13})}{A_L(\mathrm{C{=}O})} \right)_{x_z > 0.5} - \left(\frac{A_W(\nu_{13})}{A_L(\mathrm{C{=}O})} \right)_{x_z = 0.5} \right\}_{L+Z} \cdot \times \left(\frac{1 - x_z}{2 \cdot x_z - 1} \right)_{x_z > 0.5} \cdot R_{Z/L} \cdot \tag{7}$$

3. Results and discussion

3.1. IR-spectral characteristics of POPC before and after Zn^{2+}-binding

The polar moieties of POPC progressively bind water with increasing relative humidity, RH. Hydrogen-bond formation between water and the carbonyl and phosphate groups leads to a characteristic shift of the absorption bands of the C = O stretching mode, $\nu(\mathrm{C=O})$, and of several vibrational modes of the phosphate group [cf., peaks (1), (5) and (8) in Fig. 1a, and Table 1 for assignments] [21,25–27]. Two weak features at ~ 1199 and $\sim 1222\ \mathrm{cm}^{-1}$ are noted at low humidity. They are due to the $k = 1$ and $k = 2$ components of the methylene wagging band progression, $\gamma_W(CH_2)_n^k$, of the all-*trans* palmitoyl chains [28].

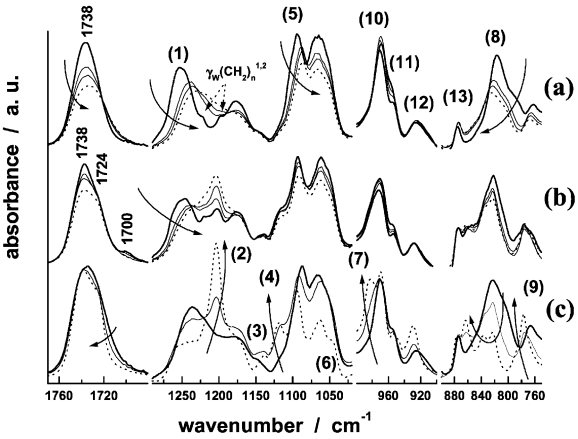

Fig. 1. Selected regions of the IR spectrum of POPC in the absence (a) and presence of Zn^{2+} (b, $R_{Z/L} = 0.7$) at variable $RH(D_2O) = 5$, 50, 71 and 89%, and at a variable molar ratio of $ZnCl_2$-to-POPC, $R_{Z/L} = 0$, 0.7 and 1 (*c*, RH = 71%). The temperature was $T = 30°C$. The arrows indicate spectral shifts which are induced either by progressive hydration (a and b) or by the binding of Zn^{2+} (c). The numbers correspond to the vibrational modes which are assigned in Table 1.

In the presence of Zn^{2+}, the spectra display a number of new absorption bands [peaks (2), (4) and (7) in Fig. 1c] which have been assigned to vibrations of the non-esterified oxygens of the PO_2^--group and of the C^G(glycerol)–O–PO_2^-–O–C^C(choline)-backbone (see Table 1). Other bands of the phosphate group sharpen [peaks (3) and (6)], decrease in intensity [peaks (1) and (8)], shift considerably [peak (9)] and split into a doublet [peak (8)]. Upon interaction of multivalent cations with the free oxygens of the phosphodiester group, the asymmetric and the symmetric PO_2^- stretching modes are known to shift considerably toward lower and higher wavenumbers, respectively [29]. The sharp, prominent feature in the spectrum of POPC/Zn^{2+} at $\sim 1204\ cm^{-1}$ (peak (2) is therefore attributed to the antisymmetric PO_2^--stretching mode of phosphate groups that interact directly with Zn^{2+}-ions. An assignment of the absorption band at 1119 cm^{-1} [peak (4)] to the corresponding symmetric mode, $\nu_s(PO_2^-)_{Zn}$, appears reasonable when the two free oxygens of the phosphinyl fragment coordinate in a symmetric bidendate manner with Zn^{2+} because the band spacing between the antisymmetric and symmetric PO_2^- modes is expected to decrease in this case [30]. The intensity of the $\nu_s(PO_2^-)$ band [peak (5)] is, however, hardly affected in the presence of zinc in contrast to the $\nu_{as}(PO_2^-)$ band [peak (1)]. Moreover, upon interaction with other dications such as Ca^{2+} the band in the 1115–1120 cm^{-1} range appears without the corresponding downwards shift of $\nu_{as}(PO_2^-)$ (manuscript in preparation). We therefore assign peak (4) to the C^G–O–(P) stretching vibration, in accordance with the literature [31,32].

We conclude that Zn^{2+} binds in an asymmetrical fashion to the PO_2^- moieties. This way, the divalent cations form bridges between neighboring phosphate groups via strong interactions with the free oxygens. Analysis of a set of independent phosphinyl–zinc complexes shows that symmetrical bidendate interaction is indeed not preferred [1,33]. Instead, the PO_2^- group tends to interact with Zn^{2+} with syn coordination stereochemistry where the average P–O...Zn^{2+} angle is 136° and the ions typically lie out of the plane which is formed by the atoms of the PO_2^- group. Zinc displays coordination number 4–6 in complexes with other molecules [1]. One can therefore suggest that other electronegative moieties such as ester oxygens and/or carbonyl groups are directly involved in complex formation with Zn^{2+}, and thus cause its high stability (vide infra).

The preferred conformations of the P–O ester bonds within the C^G–O–P–O–C^C-segment are g(auche)$^+$/g^+ or g^-/g^- [29,34]. When divalent metal ions bind to the phosphate groups of negatively charged, fully hydrated lipids such as dimyristoyl-phosphatidylserine or phosphatidic acid (DMPS or DMPA, respectively), this has been shown to result in a loss of hydration and in a conformational change from the g/g to the t(rans)/t conformation [31,35]. A similar conformational change is deduced here for the zwitterionic POPC headgroups, based on the fact that the intensities of the ν_{as}(P-(OC)$_2$) band [peak (8)] and of the C–O–P-modes [peak (3), (4), (6), (7)] show opposite tendencies upon Zn^{2+} binding. Both types of modes are expected to couple more strongly in the t/t conformation because of the coplanar arrangement of the C–O–P and the

Table 1
Assigments, wavenumbers at maximum absorption, and IR order parameters of selected vibrations of the phosphate and trimethylammonium groups of POPC in the absence and presence of Zn^{2+} [a]

Peak	Assignment[b]	Position[c] cm^{-1}	S^d_{IR}	Position[c] cm^{-1} $+Zn^{2+}$	S^d_{IR}	Transition moment[e]
Phosphate						
(1)	$\nu_{as}(PO_2^-)$	1235	−0.12	~ 1235	−0.1	
(2)	$\nu_{as}(PO_2^-)_{Zn}$	–	–	1204	−0.3	
(3)	$\nu(C^C\text{-}O(P))$	1148w	~ 0	1139	0.2	
(4)	$\nu(C^G\text{-}O(P))$	nd	–	1119	−0.1	
(5)	$\nu_s(PO_2^-)$	1090	0	1094	−0.17	
(6)	$\nu(P\text{-}O(C^C))$	sh	–	1045	−0.16	
(7)	$\nu(P\text{-}O(C^G))$	nd	–	984	0.4	
(8)	$\nu_{as}(P\text{-}(OC)_2)$	823	0.35	838, 825	0.16	
(9)	$\nu_s(P\text{-}(OC)_2)$	765	−0.21	775	−0.23	
Trimethylammonium						
(10)	$\nu_{as}(N\text{-}C)_{ip}$	969	−0.1	969	−0.2	⊥ to C-N, in-plane of CCN
(11)	$\nu_{as}(N\text{-}C)_{op}$	956sh	−0.2	955, 948	−0.05, −0.35	⊥ to C-N, out-of-plane of CCN
(12)	$\nu_s(C\text{-}N)_t$	926br	−0.05	930sp	−0.2	‖ to C-N, CC-CN is trans
(13)	$\nu_s(N\text{-}C)_g$	874	−0.2	877, 864	−0.2, −0.06	‖ to C-N, CC-CN is gauche

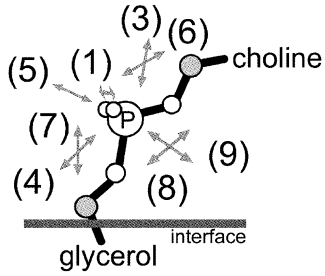

[a] Conditions: $R_{Z/L} = 0.7$, RH = 71%, T = 30°C.

[b] From [20,26,29,31,32]: ν, stretching vibration, s, symmetrical; as, antisymmetrical, $-C^G\text{-}O\text{-}PO_2^-\text{-}O\text{-}C^C$-: C^G and C^C, carbons of the glycerol and choline moieties, resp.; ip, in-plane, op, out-of-plane with respect to C-C-N; g, gauche, t, trans of the (O)-C-C-(N) fragment.

[c] Resolution ± 0.5 cm^{-1}, w, weak; nd, not detected, sh, shoulder, br, broad, sp, sharp.

[d] Calculated after baseline correction, SE ~ 0.05.

[e] The arrows schematically illustrate the direction of the transition moment of the vibration listed for the respective peaks. See text.

O–P–O fragments. We suggest that the vibrational energy of the $\nu_{as}(P\text{-}(OC)_2)$ mode partially distributes over the C–O–P stretches in the presence of Zn^{2+}, and thus its intensity weakens while that of the C–O–P modes increases. In the g/g conformation of POPC in the absence of Zn^{2+}, the intense $\nu_{as}(P\text{-}(OC)_2)$ mode can be viewed as a virtually isolated group frequency due to the non-coplanar arrangement of the C–O–P and O–P–O segments. The sharpening of the vibrational modes of the C^G–O–P–O–C^C-backbone indicates that the binding of the metal ions is accompanied by a pronounced immobilization of the PC headgroups (vide infra).

The presence of $ZnCl_2$ leads to a sharpening [peak (12), see Table 1 for assignments] and/or shift [peaks (11), (12), (13)] of the N–C stretching modes of the choline groups, whose conformation is obviously also affected by the binding of Zn^{2+} (Fig. 1c). The splitting of the $\nu_{as}(N\text{–}C)_{op}$ [peak (11)], $\nu_s(N\text{–}C)_g$ [peak (13)] and $\nu_{as}(P\text{-}(OC)_2)$ [peak (8)] modes can be attributed either to the presence of two spectroscopic species with different conformations or environments, or to a correlation field splitting resulting from the mutual interactions between highly ordered PC-headgroups.

Finally, the contour of the acyl chain C = O stretching band also sharpens in the presence of zinc ions (Fig. 1c). The shift of the right flank toward higher wavenumbers can be interpreted in terms of a Zn^{2+}-induced dehydration of the carbonyl moieties [27]. On the other side of the band a low-frequency shoulder is clearly visible at 1724 cm^{-1}, which suggests that some carbonyls are engaged in stronger interactions. They may be in direct contact with the Zn^{2+} ions, or close to other moieties that are re-structured by the bind-

ing of Zn^{2+} to the phosphate groups. For example, some water molecules could be trapped near the interface by the divalent cations and form H-bonds to the carbonyl groups [31]. A weak low-frequency feature at 1700 cm^{-1}, which appears at RH < 50%, can be explained by the same effect, i.e. by very strong C = O...HOH hydrogen bonds of immobilized water. We note that hydrogen bonded C = O groups of partly hydrolyzed PC also absorb near 1700 cm^{-1} [36]. However, such an assignment probably does not apply to the POPC + Zn^{2+} sample, because the weak feature at 1700 cm^{-1} is not detected in absence of Zn^{2+}, and moreover, it disappears at RH > 50%.

3.2. Molecular ordering of the polar groups of POPC in the presence and absence of Zn^{2+}

The lipid forms multibilayer stacks which align predominantly parallel to the ATR surface, as indicated by the negative IR order parameters of the methylene stretching bands (vide infra; [21,29]). The IR linear dichroism of selected vibrations of the PC headgroup and carbonyl groups is well suited to characterize the orientation and ordering of these segments with respect to the membrane normal, *d*, which is assumed to point parallel to the normal of the ATR surface

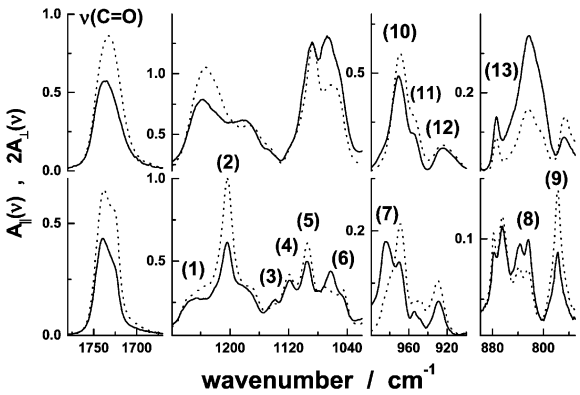

Fig. 2. Selected regions of the polarized IR spectra, $A_{\|}(\nu)$ (solid lines) and $2A_{\perp}(\nu)$ (dotted line), of POPC in the absence (above) and presence of Zn^{2+} (below, $R_{Z/L} \approx 1$) in a D_2O atmosphere of RH = 71% at $T = 30°C$. The numbers are assigned to the absorption bands of the phosphate (below) and trimethylammonium (above) groups (cf. Table 1).

[20,37–39]. Fig. 2 compares the polarized IR spectra, $A_{||}(\nu)$ and $2A_{\perp}(\nu)$, of selected spectral regions of POPC in the absence and presence of Zn^{2+}. Note that the condition $A_{||}(\nu) = 2A_{\perp}(\nu)$ refers to a random orientation of the respective transition moment, or, alternatively, to a mean inclination angle of 55° with respect to *d*. For the specification of the IR-order parameters we applied baseline correction and band separation techniques to minimize the interference with overlapping bands (data not shown, see e.g. [22]). Characteristic S_{IR}-values are given in Table 1.

The IR-order parameters of the vibrational modes of the phosphate and choline groups of POPC in the absence of Zn^{2+} are readily interpreted in terms of the accepted picture of headgroup orientation in PC membranes [20,29,40–44]. Basically, the highly mobile choline moiety, on average, orients more parallel than perpendicular to the membrane surface. The negative value of $S_{IR}(\nu_{as}(PO_2^-))$ indicates that the connecting line between the non-esterified oxygens also lies essentially parallel to the membrane (see Table 1). Likewise, the positive value of $S_{IR}(\nu_{as}(P\text{-}(OC)_2))$ suggests an oblique orientation for the esterified oxygens.

Upon Zn^{2+} binding, the IR-absorption bands of the phosphate group show pronounced changes in the linear dichroism. In particular, the big positive/negative values of $S_{IR}(\nu(P\text{-}O(C^G))/S_{IR}(\nu_{as}(PO_2^-)_{Zn})$ [peaks (7)/(2)] are compatible with a relatively uniform orientation of the corresponding transition dipoles. Consequently, this suggests a high degree of molecular ordering of the phosphate groups.

Each of the two C–O–P fragments gives rise to a doublet [i.e. peaks (3)/(6) and (4)/(7)]. The corresponding high and low frequency components can be assigned, in a simplified fashion, to virtually isolated C–O and P–O bond stretches, respectively. Alternatively, they could be assigned to antisymmetric and symmetric modes due to the coupling between the stretches of adjacent bonds (i.e. C–O–P) [32]. In the first situation the transition dipoles would point roughly along the vibrating bonds, whereas the transition dipoles of the symmetric and antisymmetric modes would orient approximately parallel and perpendicular with re-

spect to the bisector of the P–O–C bond angle. We suggest that the real situation combines both simplified views. Consequently, the transition moment of the left-hand component of each doublet is expected to deviate from the corresponding C–O bond direction toward the long axis of the C–O–P fragment. Similarly, the transition moment of the low frequency component should deviate from the P–O direction toward the bisector of the C–O–P angle. The diagram in Table 1 schematically illustrates this situation. For the t/t conformation of the two P–O ester bonds one expects alternating IR-order parameters according to the sequence $S_{IR}(\nu(C^G\text{–}O(P))) < S_{IR}(\nu(P\text{-}O(C^G))) > S_{IR}(\nu(P\text{-}O(C^C))) < S_{IR}(\nu(C^C\text{-}O(P)))$. The measured values exactly match this expectation, and thus confirm the stretched conformation of C–O–P–O–C backbone (cf. Table 1 for illustration). Note that also the S_{IR} values of the other phosphate modes [peaks (2), (5), (8), (9)] are compatible with the extended orientation of the phosphate group shown in Table 1. The negative value of $S_{IR}(\nu_{as}(PO_2^-)_{Zn})$ indicates that the O–P–O plane preferentially cuts the membrane surface at a right angle in the presence of Zn^{2+}.

The different shape of the polarized spectra $A_{\parallel}(\nu)$ and $A_{\perp}(\nu)$ in the spectral range of the $\nu(C=O)$ band confirms the multicomponent nature of this feature which has been mentioned in the previous paragraph (Fig. 2). Subbands at 1726 ± 3 and at 1740 ± 3 cm^{-1} were attributed to populations of free and hydrogen-bound C = O groups, respectively, which in turn are summations of contributions of both the *sn*-1 and *sn*-2 carbonyl moieties [27,45,46]. The polarized spectra show that the transition moments of both populations possess different orientations with respect to the bilayer normal, in agreement with recent dichroism measurements on lipid systems [47]. The orientation of the subbands is obviously not affected by the presence of zinc ions. The spectra reveal a distinct sharpening of the low frequency component. Its position remains, however, fixed at 1723 ± 1 cm^{-1}. One can conclude that the presence of Zn^{2+} reduces the width of the distribution function of interaction energies of the carbonyls, whereas its mean value remains essentially constant.

3.3. The binding equilibrium of Zn^{2+}/POPC

The ν_s(P-(OC)$_2$) band [peak (9)] represents a well resolved feature, which shifts considerably upon Zn^{2+} binding but retains a nearly constant integral absorbance. With $g \approx 1$ Eq. (2) becomes $x_A \approx (COG - COG_B)/(COG_A - COG_B)$. Hence, the center of gravity, COG(ν_s(P-(OC)$_2$)) provides a suitable probe to estimate the mole fraction of lipid molecules whose phosphate groups interact strongly with Zn^{2+}, $x_{LZ} = N_{LZ}/N_L^t \approx (COG\text{–}COG_{min})/(COG_{max}\text{–}COG_{min})$. COG_{max} and COG_{min} denote the minimum and maximum values which correspond to free and Zn^{2+}-bound phosphate groups, respectively. The fraction x_{LZ} increases linearly with the addition of Zn^{2+} according to $x_{LZ} \approx 2 \cdot x_z$, and it reaches a 'plateau'

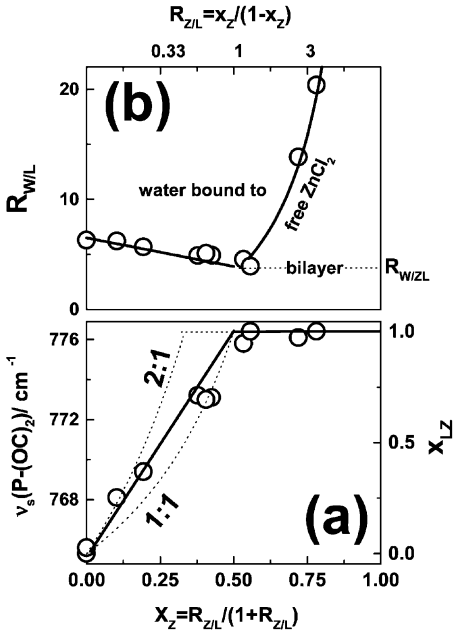

Fig. 3. Center of gravity of the ν_s(P-(OC)$_2$) band of POPC (part a) and the number of water molecules per lipid, $R_{W/L}$ (part b, see below), as a function of the mole fraction of $ZnCl_2$, x_z, at RH = 71%. $R_{W/L}$ has been estimated from the integrated intensity of the ν_{13}(OD) band of water (see below). The right axis in part (a) gives the mole fraction of the lipid–zinc complex x_{LZ}. The dotted lines in part (a) refer to a 2:1 (lipid:Zn^{2+}) and 1:1 stoichiometry of the complex [see Appendix A, Eq. (A5)]. The solid lines refer to the model of strong binding (cf. Appendices A and B).

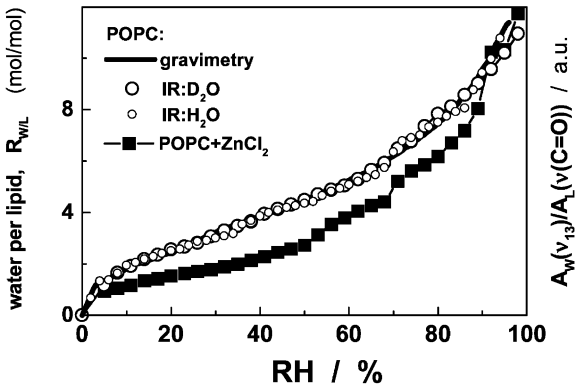

Fig. 4. Gravimetrically determined molar ratio of water-to-lipid ($R_{W/L}$, solid line, H_2O [48]), and the ratio of the integrated intensities of the ν_{13} and ν(C = O) bands (A_W/A_L, symbols, H_2O and D_2O) of POPC as a function of relative humidity (RH). The solid squares show the respective adsorption isotherm of POPC in the presence of $ZnCl_2$ ($R_{Z/L} = 0.7$). Maximum agreement between the gravimetric and IR isotherms was achieved when a constant amount of 0.8 water molecules per lipid was added to the gravimetric data. This correction can be explained by imperfect drying of the sample in the gravimetric experiment.

at $x_Z > 0.5$ (Fig. 3a). The saturation behavior is consistent with a 1:1 binding stoichiometry, similar to the complex between Ca^{2+} and the doubly charged PO_3^{2-} groups of DMPA [31]. The Ca^{2+}-complex has been described as a two-dimensional network, where lipids within the same (*cis*) and between opposite (*trans*) bilayers are bridged by the divalent metal-ions, each of which appears to be coordinated by four lipids, and each lipid by four ions. Note that the initial behavior of the binding of Zn^{2+}, however, is more compatible with the formation of a 2:1 complex of POPC:Zn^{2+} (see Fig. 3 and Appendix A).

The binding of Zn^{2+} is accompanied by a considerable dehydration of the uncharged lipid (see Section 3.4). For example, at RH = 71%, the number of water molecules per lipid is reduced from $R_{W/L} \approx 6.5$ in the absence of Zn^{2+} to $R_{W/L} \approx 4$ at $R_{Z/L} \approx 1$ (Fig. 3b). The Zn^{2+} ions obviously replace the primary hydration shell of the phosphate groups to some extent. A similar effect was reported for the interaction of cations with charged phospholipids [35]. Beyond the saturation limit, i.e. at $x_Z > 0.5$, the solvation of 'free' $ZnCl_2$ gives rise to a drastic increase of the amount of adsorbed water (Fig. 3b).

It is difficult to assess the partitioning of Zn^{2+} between its 'free' solvated form and its bound state at the partially hydrated zwitterionic POPC headgroup. An appropriate model must consider both the binding and saturation behavior (Fig. 3a) as well as the hydration (Fig. 3b) of the system. Models which treat the data in terms of a binding equilibrium of a fixed stoichiometry and a finite value of the binding constant are found to overestimate the amount of adsorbed water at $x_Z < 0.5$, because they predict a certain fraction of free, hygroscopic Zn^{2+} (not shown). In Appendices A and B we present a simple, alternative model. It assumes strong binding at $x_Z < 0.5$ and saturation of the lipid with Zn^{2+} at $x_Z > 0.5$. It

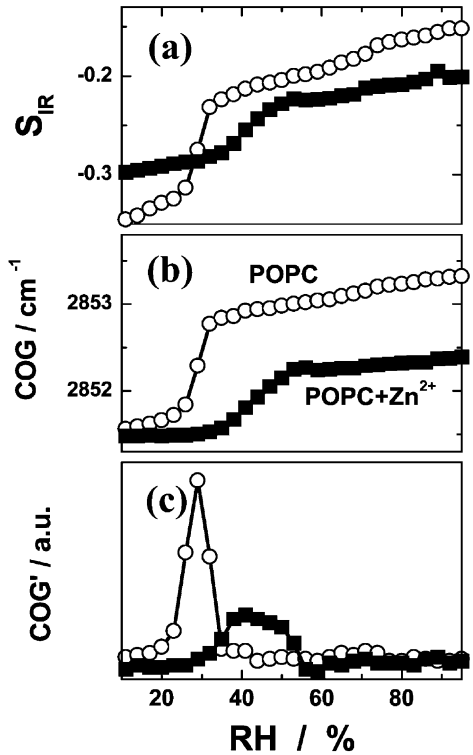

Fig. 5. IR order parameter, S_{IR} (part a), center of gravity, COG (part b), of the methylene stretching vibration and its first derivative, COG′ (part c), of POPC and of POPC + Zn^{2+} ($R_{Z/L} = 0.7$) as a function of the relative humidity, RH, at $T = 30°C$.

readily explains the experimental data in the intermediate RH range (50% < RH < 85%, e.g. Fig. 3). The primary hydration shell of the PC headgroup is usually complete at these water activities [48]. For the hydration capacity of pure $ZnCl_2$ we used $R_{W/Z} = 7.0 \pm 0.5$ [RH = 71%, cf. Eq. (B5)]. This value was independently determined gravimetrically. At low humidity (RH < 50%) and at high Zn^{2+}-concentrations ($R_{Z/L} > 0.85$) the phosphate/Zn^{2+} complex partially decomposes (see Section 2). This behavior indicates that the PO_2^-/Zn^{2+} interactions are stabilized in the presence of water.

In summary, the water adsorption characteristics and the spectral response of the phosphate groups demonstrate that zinc cations strongly bind to the phosphate moieties of POPC. The apparent stoichiometry of the initial Zn^{2+} binding is 2:1 POPC:Zn^{2+}, whereas at saturation each lipid binds approximately one Zn^{2+}-ion.

3.4. Water binding characteristics

Fig. 4 compares the adsorption isotherm of POPC (cf. [48]) with the ratio of the integrated intensities, $A_W(\nu_{13})/A_L(C=O)$, as a function of RH [cf. Eq. (6)]. The hydration of the lipid with D_2O and H_2O yields identical curves, in agreement with previous results [49]. This spectroscopic parameter is obviously well-suited to monitor the binding of water to the lipid (see also [19,25,39]).

The normalized IR absorption band of water in the different systems was transformed into an $R_{W/L}$-scale using Eq. (6). Fig. 4b shows that the lipid becomes considerably less hydrated in the presence of $ZnCl_2$. It should be taken into account that the water binding capacity of Zn^{2+}, too, is distinctly reduced in the presence of the lipid due to complex formation. For example, one mole of pure lipid and one mole of pure $ZnCl_2$ take up ~7 mol of water each at RH ≈ 71%. The mixture of both components ($R_{Z/L} = 0.7$) binds merely $R_{W/L} \approx 5$ water molecules per lipid. This difference in water-binding capacity, $R^{exc}_{W/L}$, reflects the strong interactions between lipid and Zn^{2+} [cf. Appendix B, Eqs. (B6) and (B7)]. For example, $R^{exc}_{W/L}(L+Z) \approx -9$ (cf. Table 2), which indicates that both lipid and Zn^{2+} sacrifice more than 50% of their hydration shell upon complex formation.

Using the adsorption isotherms and the differences in water-binding capacities [cf. Eq. (B7)], it is possible to calculate the Gibbs free energy which drives the hydration process, according to [44,50]

$$G_{\mathrm{dehyd}}(R_{\mathrm{W/L}}) = RT \cdot \int_{a_w=1}^{a_w} \ln a_w \cdot \mathrm{d}R_{\mathrm{W/L}}(a_{\mathrm{W}}) \quad (8)$$

and the excess Gibbs free energy of dehydration of the mixtures [see also Eq. (B7)]

$$G^{\mathrm{exc}}_{\mathrm{dehyd}}(R_{W/L}) \equiv G_{\mathrm{dehyd}} - G^{\mathrm{id}}_{\mathrm{dehyd}} = RT \cdot \int_{a_w=1}^{a_w} \ln a_w \cdot dR^{\mathrm{exc}}_{W/L}(a_W) \quad (9)$$

The Gibbs free energy of dehydration, G_{dehyd} represents a measure of the work to remove water from the fully hydrated system to a reduced water activity of $a_{\mathrm{w}} = \mathrm{RH}/100\% < 1$ [50]. G_{dehyd} can be fairly well approximated over a wide range of $R_{W/L}$ by an exponential function, $G_{\mathrm{dehyd}}(R_{W/L}) \approx G^0_{\mathrm{dehyd}} \cdot \exp(-R_{W/L}/R^0_{W/L})$ which yields the Gibbs free energy of complete dehydration, G^0_{dehyd}, and a characteristic number of 'tightly

Table 2
Thermodynamic and structural data on the hydration of lipid/peptide/Zn^{2+} systems[a]

System	G^0_{dehyd} kJ/mol	$R^0_{\mathrm{W/L}}$	$G^{\mathrm{exc}}_{\mathrm{dehyd}}(0)$ kJ/mol	$R^{\mathrm{exc}}_{\mathrm{W/L}}$ at RH = 71%
POPC	26	2.5		
POPC + Zn^{2+}	16	2.6	−24	−9

[a] Errors: ±2 kJ/mol (G^0_{dehyd},$G^{\mathrm{exc}}_{\mathrm{dehyd}}$), ±0.2 ($R^0_{\mathrm{W/L}}$), ±1 ($R^{\mathrm{exc}}_{\mathrm{W/L}}$).

bound' water molecules, $R^0_{W/L}$ (Table 2). The presence of Zn^{2+} reduces G^0_{dehyd} by ~10 kJ/mole when compared with pure POPC. The absolute value of the corresponding excess Gibbs free energy of complete dehydration, $G^{exc}_{dehyd}(0)$ is of the order of the Gibbs free energy of complete dehydration of the lipid, G^0_{dehyd}.

G_{dehyd} can be regarded as a measure of the energetic cost of pushing two bilayers together to a water gap between them which consists of $2R_{W/L}$ water molecules per lipid. Consequently, G^0_{dehyd} represents a measure of two bilayers to come into contact. The close approach and subsequent fusion of lipid bilayers in excess water requires partial dehydration of the lipids in the region of contact. Hence, the marked decrease of G^0_{dehyd} in the presence of Zn^{2+} can be viewed as the thermodynamic driving force of zinc-induced fusion. The accompanying decrease in the number of tightly bound water molecules per lipid can be interpreted as a reduction in the repulsive 'hydration' forces, which usually prevent the spontaneous fusion of lipid vesicles.

3.5. The effect of Zn^{2+} on the lyotropic chain melting transition of POPC

Fig. 5 shows the center of gravity, COG, and the IR order parameter, S_{IR}, of the symmetric methylene stretching band, $\nu_s(CH_2)$, of POPC in the presence and absence of Zn^{2+} upon decreasing the relative humidity, RH, of the vapor atmosphere. The sigmoidal decrease of both spectral parameters, $S_{IR}((\nu_s(CH_2))$ and $COG(\nu_s(CH_2))$, is typical for the lyotropic liquid–crystalline/gel phase transition [21]. The freezing of the acyl chains into a predominantly stretched all-*trans* conformation is evident from the existence of the CH_2 wagging band progression at small RH (see Fig. 1).

The position and width of the phase transition can be well characterized from the first derivative $COG' = \delta COG(\nu_s(CH_2))/\delta RH)$. The divalent ions stabilize the gel state of the lipid bilayer, because the center of the transition is shifted to a higher value of RH by $\Delta RH \approx 15\%$. The IR parameter, $S_{IR}(\nu_s(CH_2))$ and the mean position, $COG(\nu_s(CH_2))$, suggest that the hydrophobic core in the L_α-phase is more ordered in the presence of Zn^{2+} than compared with pure POPC. This tendency can be explained by the formation of Zn^{2+}-bridges, which connect the phosphate groups of adjacent lipids and thereby reduce the molecular area available to the acyl-chains in the L_α-phase [51]. These results are in good agreement with the effects on the thermotropic chain melting transition of phospholipid membranes that have been described for other divalent metal ions [31,35,52]. Recently, we showed that the hydration induced shift of the $\nu_s(CH_2)$ band represents a measure of the lateral compressibility of lipid membranes [53]. Consequently, the significantly smaller slope COG′ outside the phase transition range in the presence of Zn^{2+} indicates that the membranes become less compressible due to the Zn^{2+}-bridges.

The width of the lyotropic phase transition of POPC is also found to be markedly increased in the presence of zinc, possibly due to a microheterogeneous distribution of Zn^{2+}–lipid complexes and of virtually free lipid. Note that the additional degree of thermodynamic freedom in the three-component mixture (free POPC + POPC-Zn^{2+}–complex + water) is compatible with a transition over a range of RH, according to Gibbs phase rule of a first order transition at $T = \text{const}$ and $p = \text{const}$. With increasing $R_{Z/L}$ the amount of lipid not involved into complex formation is expected to decrease. Indeed, the chain melting transition disappears nearly completely at a Zn^{2+}–lipid molar ratio near unity indicating saturation of the complex (not shown). Under these conditions Zn^{2+} stabilizes POPC in the gel state over the full hydration range studied.

3.6. The polar region of the membranes as a function of hydration

The continuous change of the center of gravity, COG, of selected stretching bands of the carbonyl and phosphate groups of POPC with increasing RH are characteristic signatures of the progressive hydration of the polar moieties of POPC (cf. Fig. 6). The addition of Zn^{2+} shifts $COG(\nu_{as}(PO_2^-))$ to lower wavenumbers due to the spectral overlap with the $\nu_{as}(PO_2^-)_{Zn}$-band which

interferes with the $\nu_{as}(PO_2^-)$ mode in the spectral range $> 1210\ cm^{-1}$ (see Fig. 1). At the same time the $COG(\nu_{as}(P\text{-}(OC)_2))$ is shifted to higher wavenumbers because of the conformational change of the phosphate group (Fig. 6d). The position of the $\nu_{as}(PO_2^-)_{Zn}$ band in the presence of Zn^{2+} is virtually independent of RH, in contrast to the behavior of the $\nu_{as}(PO_2^-)$-mode of pure POPC [compare peaks (1) and (2) in Fig. 1b]. The ability of the Zn^{2+}-bound phosphate groups to take up water is obviously reduced, meaning that the headgroups have become less hydrophilic.

The $COG(\nu_s(PO_2^-))$ values of POPC and of the POPC/Zn^{2+} complex are nearly equal at RH < 10% (cf. Fig. 6c). With increasing RH the phosphate groups become more strongly hydrated in the absence of Zn^{2+} than in its presence, as indicated by the more negative slope of $COG(\nu_s(PO_2^-))$ vs. RH. This effect can be attributed to the ability of Zn^{2+} to screen the phosphate groups from water. The $COG(\nu(C=O))$ data can be interpreted in an analogous fashion (Fig. 6a). The drop of $COG(\nu(C=O))$ of the POPC + Zn^{2+} sample at RH < 55% suggests that Zn^{2+} may be able to interact directly with the carbonyl groups at low levels of hydration. A similar dehydration of the carbonyl, and especially of the phosphate groups of DMPC, has been previously reported to occur after the addition of divalent Ca^{2+} [36].

The IR order parameter of the $\nu(C=O)$ and $\nu_{as}(P\text{-}(OC)_2)$ bands (Fig. 6e,h) change markedly at the lyotropic melting transition of the lipid, whereas $S_{IR}(\nu_{as}(PO_2^-))$ and $S_{IR}(\nu_s(PO_2^-))$ are almost insensitive to this event (Fig. 6f,g). This different behavior shows that the degree of macroscopic ordering of the bilayers is virtually unaffected by the phase state of the lipid and/or by the composition of the samples. The drop in the absolute values of $S_{IR}(\nu(C=O))$ and $S_{IR}(\nu_{as}(P\text{-}(OC)_2))$ at the chain melting transition can be attributed to the gradual disordering of the carbonyl and phosphate groups. The extremely different responses of $S_{IR}(\nu_{as}(P\text{-}(OC)_2))$ and of $S_{IR}(\nu_{as}(PO_2^-))$ show that the mean orientation of the phosphate groups is modified in an anisotropic fashion. The CO–P–OC backbone seems to align more parallel with respect to the membrane surface in the L_α phase, possibly be-

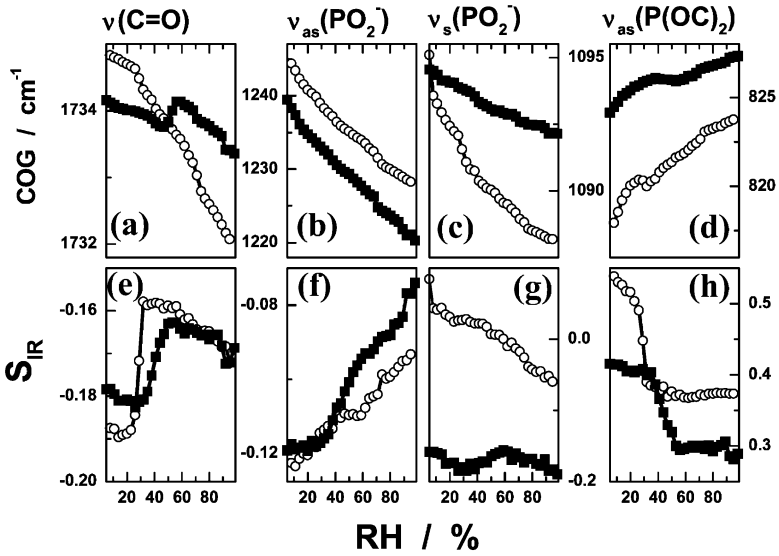

Fig. 6. IR order parameter, S_{IR} (below), center of gravity, COG (above), of the carbonyl (part a and e), the antisymmetric and symmetric PO_2^- (part b, c and f, g) and the antisymmetric $P\text{-}(OC)_2$ (part d and h) stretching vibrations (from left to right, see symbols) of POPC and POPC + Zn^{2+} as a function of the relative humidity, RH, at $T = 30°C$.

cause of the expansion in membrane area which typically accompanies the lipid melting transition.

3.7. Partly covalent nature of zinc binding to phosphodiester groups

Like all metal cations, Zn^{2+} interacts electrostatically with anionic groups. In contrast to other divalent metal cations with similar ionic radius such as Mg^{2+} zinc ions possess a higher affinity to electronegative groups [8]. Zn^{2+} obviously binds more tightly. For example, the interaction between nucleobases and Zn^{2+} possesses partly the characteristics of a covalent bound in metalated bases than of coulombic interactions between charged groups [8]. This property is due to the attractive $3d^{10}$ electron-lone pair interaction of zinc which is absent for divalent alkali earth metal ions.

Moreover, theoretical calculations demonstrate a high flexibility in the modes of binding of hydrated Zn^{2+} owing to the variable hydration shell around the ion [8,54]. Zinc displays coordination number 4–6 in small-molecule complexes and the coordination number 5 is particularly common. In aqueous solution zinc exists mainly as the hexahydrate $Zn^{2+}(OH_2)_6$ [1]. As a d^{10} metal ion, Zn^{2+} is not subject to ligand field stabilization effect, so that the change from the ligand field of hexaaqueo species $Zn^{2+}(OH_2)_6$ to a ligand–Zn^{2+} complex of different coordination number is not energetically unfavorable in contrast to other first-row transition metal ions such as Fe^{2+} and Cu^{2+} [1].

The complex consisting of hydrated phosphodiester groups of the lipid, $(P + H_2O)$, and hydrated Zn^{2+} ions, $(Z + H_2O)$, can be viewed following two approaches: (i) as a complex between the two hydrated subsystems, $(P + H_2O)$–$(Z + H_2O)$ and (ii) as a hydrated metalated phosphate group, $(P\text{-}Z) + H_2O$. The results show that the interaction of phospholipid headgroups with Zn^{2+} is more conveniently described by the second interpretation. In other words, the situation can be partly described by the shift of an interaction between hydrated phosphates and hydrated cations towards the hydration of a zinc–phosphate complex the key energy contribution of which is more covalent in nature.

4. Summary and conclusions

The main aim of this study was to characterize the effect of Zn^{2+} on the headgroup structure, hydration and phase behavior of POPC. Our results can be summarized as follows.

Zinc ions interact strongly with the polar groups of the zwitterionic lipid, and in particular with the negatively charged phosphate groups. The formation of a 2:1–1:1 — POPC:Zn^{2+} complex is accompanied by a conformational change of the C–O–P–O–C–backbone from a *gauche / gauche* into the *trans / trans* conformation. It appears that Zn^{2+}-bridges between neighboring lipid molecules stabilize the gel phase of the lipid relative to the liquid–crystalline state.

Furthermore, drastic dehydration of the lipids and metal cations is observed, both of which lose roughly 50% of their primary hydration shell. The energetic cost (on the scale of Gibbs free energy) for completely dehydrating the lipid headgroups is decreased by approximately 10 kJ/mole in the presence of Zn^{2+}. Dehydration of phospholipid headgroups due to complexation with zinc cations is suggested to increase fusogenic potency of lipid membranes. In other words, binding of Zn^{2+} effectively renders the membrane surface more hydrophobic, thus allowing fusion to proceed. A comparative study on the interaction of a series of alkali earth and transition metals with the zwitterionic phospholipid is now in progress to specify the hydration properties of the respective metalated phosphate groups.

Clearly, the biological effect of Zn^{2+} on phospholipid membranes depends on two events, namely accumulation near the membrane surface and formation of a stable complex with the headgroups. Membranes of anionic lipids are typically more strongly affected by metal cations than membranes of zwitterionic lipids because of stronger attractive coulombic forces. It is well known that the binding of divalent metal ions to negatively charged lipids causes rigidization of the

bilayers and dehydration of the lipid headgroups [31,35,36,52,55]. The new data presented here show that Zn^{2+} can nonetheless interact strongly with the lipid headgroup by binding directly to its phosphate group. The specific effect of zinc on biological membranes is obviously not related to the net charge of the lipid.

Enzymes that process phospholipids have received extensive attention owing to their involvement in cellular signal transduction in mammalian cells [5]. Members of the phospholipase C class catalyze the hydrolysis of phospholipids into diacylglycerol and a phosphorylated headgroup. Interestingly, the phosphatidylcholine-preferring phospholipase C has an unusual three-metal center of three zinc ions at its active site which are thought to interact directly with the phosphate group of PC lipids [6,56]. Here the specific affinity of zinc for phospholipid headgroups is probably involved in catalytic activity, and thus it represents an further example of the biological role of Zn^{2+}–phospholipid interactions.

Acknowledgements

This work was supported by the Deutsche Forschungsgemeinschaft within SFB 294 (TP C7) and SFB 197 (TP A10 and TP B13).

Appendix A: Stoichiometry of the binding of Zn^{2+} to POPC

Let us first consider a binding equilibrium of metal ions (Z) and lipid (L), according to

$$n \cdot L(\text{free}) + Z(\text{free}) \overset{K_b}{\leftrightarrow} L_n Z(\text{complex}) \tag{A1}$$

The stoichiometry (n:1) of the binding and the conservation law of matter give rise to the following relations

$$N_{LZ} = N_L^b = n \cdot N_Z^b \tag{A2}$$

$$N_L^t = N_L^b + N_L^f \quad \text{and} \quad N_Z^t = N_Z^b + N_Z^f \tag{A3}$$

The subscripts refer to the species (L, LZ and Z) and the superscript to total (t), bound (b) and free (f) lipid and Zn^{2+}, respectively (in moles, N). The water activity of saturated aqueous $ZnCl_2$ solution corresponds to RH ≈ 10% [57]. Hence, the existence of precipitated salt can be excluded from the considerations at RH > 10% under equilibrium conditions. Insertion of Eq. (A2) into

$$x_{LZ} = \frac{N_L^b}{N_L^t} \tag{A4}$$

yields the fraction of bound lipid, x_{LZ}, in the case of strong binding ($K_b \to \infty$)

$$x_{LZ} = \left\{ \begin{array}{ll} n \cdot \dfrac{x_Z}{1 - x_Z} & \text{for } x_Z < \dfrac{1}{1+n} \\ 1 & \text{for } x_Z \geq \dfrac{1}{1+n} \end{array} \right\} \tag{A5}$$

as a function of the mole fraction of zinc, $x_Z = N_Z^t/(N_Z^t + N_L^t) = R_{Z/L}/(1 + R_{Z/L})$, or alternatively, of the molar ratio of zinc-to-lipid, $R_{Z/L} = N_Z^t/N_L^t = x_Z/(1 - x_Z)$. According to Eq. (A5) the empirical function

$$x_{LZ} = \begin{cases} 2 \cdot x_Z & \text{for } x_Z < 0.5 \\ 1 & \text{for } x_Z \geq 0.5 \end{cases} \tag{A6}$$

is equivalent to a concentration-dependent stoichiometry

$$n = \begin{cases} 2 \cdot (1 - x_Z) & \text{for } x_Z < 0.5 \\ 1 & \text{for } x_Z \geq 0.5 \end{cases} \tag{A7}$$

The behavior of the (hydrated) POPC/$ZnCl_2$-mixture is summarized in terms of a phase diagram which depicts the fraction of bound and free Zn^{2+} as a function of the mole fraction of total Zn^{2+} (cf. Fig. 7).

Appendix B: Hydration of the sample

In the POPC/$ZnCl_2$ mixture the water potentially adsorbs to free lipid (superscript L), free

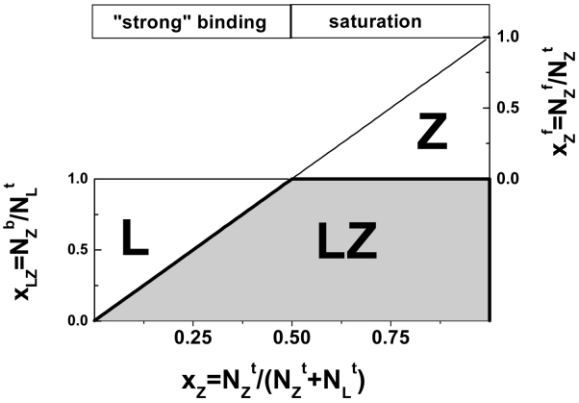

Fig. 7. Phase diagram of the POPC/$ZnCl_2$-mixture (partially hydrated, RH = 71%, T = 30°C).

Zn^{2+} (Z) and to the complex (LZ). In the case of ideal behavior the water distributes between the components, i.e.

$$N_W^t = N_W^L + N_W^Z + N_W^{LZ} \tag{B1}$$

The latter two terms are assumed to include the hydration of the respective amount of Cl^- counterions. Division by the total moles of lipid, N_L^t, and making use of the molar ratios

$$\begin{aligned} &R_{W/L} = N_W^t/N_L^t;\ R_{W/L}(L) = N_W^L/N_L^f; \\ &R_{W/LZ} = N_W^{LZ}/N_L^b;\ R_{W/Z}(Z) = N_W^Z/N_Z^f \end{aligned} \tag{B2}$$

yields

$$\begin{aligned} R_{W/L} = N_L^{t-1}\cdot\Big(&R_{W/L}(L)\cdot N_L^f + R_{W/LZ}\cdot N_L^b \\ &+ R_{W/Z}(Z)\cdot N_Z^f\Big) \end{aligned} \tag{B3}$$

After insertion of Eqs. (A2) and (A4) this equation is rewritten as

$$\begin{aligned} R_{W/L} = &R_{W/L}(L)\cdot(1-x_{LZ}) + R_{W/LZ}\cdot x_{LZ} \\ &+ R_{W/LZ}(Z)\cdot\left(R_{Z/L} - \frac{x_{LZ}}{n}\right) \end{aligned} \tag{B4}$$

Within the framework of the model of strong binding (Eqs. (A6) and (A7)) no free Zn^{2+} contributes to the hydration of the sample at $x_Z < 0.5$, whereas in the saturation range above $x_Z \geq 0.5$ the water adsorption is determined by free Zn^{2+}, according to

$$R_{W/L} = \begin{cases} R_{W/L}(L)\cdot(1-2x_Z) + 2\cdot R_{W/LZ}\cdot x_Z;\ x_Z < 0.5 \\ R_{W/LZ} + R_{W/Z}(Z)\cdot\dfrac{2\cdot x_Z - 1}{1-x_Z};\quad x_Z \geq 0.5 \end{cases} \tag{B5}$$

Note that at $x_Z < 0.5$ the system is treated as a two-component ideal mixture of the 'free' lipid and the complex. At $x_Z \geq 0.5$ the complex and 'free' dissociated $ZnCl_2$ can be viewed as two separate phases.

Let us now consider the hydration of the quasi-binary system POPC/$ZnCl_2$. Following the same formalism as above one obtains in the case of ideal behavior

$$R_{W/L}^{\mathrm{id}}(L+Z) = R_{W/L}(L) + R_{W/Z}(Z)\cdot R_{Z/L} \tag{B6}$$

The excess amount of adsorbed water per lipid in the real mixtures is defined by

$$R_{W/L}^{\mathrm{exc}} = R_{W/L} - R_{W/L}^{\mathrm{id}} \tag{B7}$$

Comparison of Eqs. (B5) and (B7) yields $R_{W/L}^{\mathrm{exc}}(L+Z) = R_{W/LZ}\text{-}(R_{W/L}(L) + R_{W/Z}(Z))$ at $x_Z = 0.5$ [see also Eq. (7)].

References

[1] D.W. Christianson, Structural biology of zinc, Adv. Protein Chem. 42 (1991) 281–355.
[2] U. Ryde, Carboxylate binding modes in zinc proteins: a theoretical study, Biophys. J. 77 (1999) 2777–2787.
[3] C. Tu, M. Qian, J.N. Earnhardt, P.J. Laipis, D.N. Silverman, Properties of intramolecular proton transfer in carbonic anhydrase III, Biophys. J. 74 (1998) 3182–3189.
[4] W.N. Lipscomb, N. Sträter, Recent advances in zinc enzymology, Chem. Rev. 96 (1996) 2375–2433.
[5] J.C. Exton, New developments in phospholipase D, Eur. J. Biochem. 243 (1997) 10–20.
[6] E. Hough, L.K. Hansen, B. Birkness et al., High-resolution (1.5 A) crystal structure of phospholipase C from *Bacillus cereus*, Nature 338 (1989) 357–360.

[7] M. Kawahara, N. Arispe, Y. Kuroda, E. Rojas, Alzheimer's disease amyloid beta-protein forms Zn^{2+}-sensitive, cation-selective channels across excised membrane patches from hypothalamic neurons, Biophys. J. 73 (1997) 67–75.

[8] N. Gresh, J. Sponer, Complexes of pentahydrated Zn^{2+} with guanine, adenine, and the guanine–cytosine and adenine–thymine base pairs. Structures and energies characterized by polarizable molecular mechanics and ab inition calculations, J. Phys. Chem. B 103 (1999) 11415–11427.

[9] H. Binder, K. Arnold, A.S. Ulrich, O. Zschörnig, The effect of Zn^{2+} on the secondary structure of a histidine-rich fusogenic peptide and its interaction with lipid membranes, Biochim. Biophys. Acta 1468 (2000) 345–358.

[10] R.W. Glaser, M. Grüne, C. Wandelt, A. Ulrich, Structure analysis of a fusogenic peptide sequence from the sea urchin fertlization protein bindin, Biochemistry 38 (1999) 2560–2569.

[11] A. Hofmann, C.G. Glabe, Bindin, a multifunctional sperm ligand and the evolution of new species, Semin. Dev. Biol. 5 (1994) 233–242.

[12] V.D. Vacquier, W.J. Swanson, M.E. Hellberg, What have we learned about sea urchin sperm bindin? Dev. Growth Differ. 37 (1995) 1–10.

[13] K.D. Barfield, D.R. Bevan, Fusion of phospholipid vesicles induced by Zn^{2+}, Cd^{2+} and Hg^{2+}, Biochem. Biophys. Res. Com. 128 (1985) 389–395.

[14] M. Deleers, J.-P. Servais, E. Wulfert, Synergistic effects of micromolar concentrations of Zn^{2+} and Ca^{2+} on membrane fusion, Biochem. Biophys. Res. Com. 137 (1986) 101–107.

[15] G.A. Howell, M.G. Welch, C.J. Frederickson, Stimulation-induced uptake and release of zinc in hippocampal slices, Nature 308 (1984) 736–738.

[16] R. Lehrmann, J. Seelig, Adsorption of Ca^{2+} and La^{3+} to bilayer membranes: measurement of adsorption enthalpy and binding constant with titration calorimetry, Biochim. Biophys. Acta 1189 (1994) 89–95.

[17] P. Garidel, A. Blume, W. Hübner, A Fourier transform infrared spectroscopic study of the interaction of alkaline earth cations with the negatively charged phospholipid 1,2-dimyristoyl-*sn*-glycero-3-phosphoglycerol, Biochim. Biophys. Acta 1466 (2000) 245–259.

[18] K. Arnold, in: R. Lipowski, E. Sackmann (Eds.), Handbook of Biological Physics, Elsevier Science BV, 1995, pp. 903–957.

[19] H. Binder, A. Anikin, B. Kohlstrunk, G. Klose, Hydration induced gel states of the dienic lipid 1,2-bis(2,4-octadecanoyl)-*sn*-glycero-3-phosphorylcholine and their characterization using infrared spectroscopy, J. Phys. Chem. B 101 (1997) 6618–6628.

[20] H. Binder, T. Gutberlet, A. Anikin, G. Klose, Hydration of the dienic lipid dioctadecadienoylphosphatidylcholine in the lamellar phase — an infrared linear dichroism and X-ray study on headgroup orientation, water ordering and bilayer dimensions, Biophys. J. 74 (1998) 1908–1923.

[21] H. Binder, A. Anikin, G. Lantzsch, G. Klose, Lyotropic phase behavior and gel state polymorphism of phospholipids with terminal diene groups. Infrared measurements on molecular ordering in lamellar and hexagonal phases, J. Phys. Chem. B 103 (1999) 461–471.

[22] H. Binder, H. Schmiedel, Infrared dichroism investigations on the acyl chain ordering in lamellar structures I. The formalism and its application to polycrystalline stearic acid, Vib. Spectrosc. 21 (1999) 51–73.

[23] N.J. Harrick, Internal Reflection Spectroscopy, Wiley, New York, 1967.

[24] R.G. Snyder, M. Maroncelli, H.L. Strauss, V.M. Hallmark, Temperature and phase behavior of infrared intensities: the poly(methylene) chain, J. Phys. Chem. 90 (1986) 5623–5630.

[25] W. Pohle, C. Selle, H. Fritzsche, H. Binder, Fourier transform infrared spectroscopy as a probe for the study of the hydration of lipid self-assemblies. I. Methodology and general phenomena, Biospectroscopy 4 (1998) 267–280.

[26] J.L.R. Arrondo, F.M. Goni, J.M. Macarulla, Infrared spectroscopy of phosphatidylcholines in aqueous suspensions. A study of the phosphate group vibrations, Biochim. Biophys. Acta 794 (1984) 165–168.

[27] A. Blume, W. Hübner, G. Messner, Fourier transform infrared spetroscopy of 13C = O-labeled phospholipids. Hydrogen bonding to carbonyl groups, Biochemistry 27 (1988) 8239–8249.

[28] L. Senak, D. Moore, R. Mendelsohn, CH_2 wagging progressions as IR probes of slightly disordered phospholipid acyl chain states, J. Phys. Chem. 96 (1992) 2749–2754.

[29] U.P. Fringeli, H.H. Günthard, Infrared membrane spectroscopy, Mol. Biol. Biochem. Biophys. 31 (1981) 270–332.

[30] H.N. Halladay, M. Petersheim, Optical properties of Tb^{3+}–phospholipid complexes and their relation to structure, Biochemistry 27 (1988) 2120–2126.

[31] G. Laroche, E.J. Dufourc, J. Dufourcq, M. Pezolet, Structure and dynamics of dimyristoylphosphatidic acid/calcium complexes by 2H NMR, infrared, and Raman spectroscopies and small-angle X-ray diffraction, Biochemistry 30 (1991) 3105–3114.

[32] Tuchtenhagen, J. 1994. PhD Thesis. Kaiserslautern, Kaiserslautern

[33] R.S. Alexander, Z.F. Kanyo, L.F. Chirlian, D.W. Christianson, Stereochemistry of phosphate–Lewis acid interaction: implication for nucleic acid structure and recognition, J. Am. Chem. Soc. 112 (1990) 933–937.

[34] H. Hauser, W. Guyer, M. Spiess, I. Pascher, S. Sundell, The polar group conformation of a lysophosphatidylcholine analogue in solution — a high-resolution magnetic resonance study, J. Mol. Biol. 137 (1980) 265–282.

[35] H.L. Casal, H.H. Mantsch, H. Hauser, Infrared studies of fully hydrated saturated phosphatidylserine bilayers .

effect of Li^+ and Ca^{2+}, Biochemistry 26 (1987) 4408–4416.

[36] E. Müller, A. Giehl, G. Schwarzmann, K. Sandhoff, A. Blume, Oriented 1,2-Dimyristoyl-*sn*-glycero-3-phosphorylcholine/ganglioside membranes: a fourier transform infrared attenuated total reflection spectroscopic study. Band Assignments, orientational, hydrational, and phase behavior; and effects of Ca^{2+} binding, Biophys. J. 71 (1996) 1400–1421.

[37] H. Binder, B. Kohlstrunk, Infrared dichroism investigations on the acyl chain ordering in lamellar structures II. The effect of diene groups in membranes of dioctadecadienoylphosphatidylcholine, Vib. Spectrosc. 21 (1999) 75–95.

[38] W. Hübner, H.H. Mantsch, Orientation of specifically 13C = O labeled phosphatidylcholine multilayers from polarized attenuated total reflection FT-IR spectroscopy, Biophys. J. 59 (1991) 1261–1272.

[39] E. Okamura, J. Umemura, T. Takenaka, Orientation studies of hydrated dipalmitoylphosphatidylcholine multibilayers by polarized FTIR-ATR spectroscopy, Biochim. Biophys. Acta 1025 (1990) 94–98.

[40] P.L. Yeagle, Phospholipid headgroup behavior in biological assemblies, Acc. Chem. Res. 11 (1978) 321–327.

[41] J.L. Browning, Motions and interactions of phospholipid head groups at the membrane surface. 1. Simple alkyl head groups, Biochemistry 20 (1981) 7144–7151.

[42] D.M. Small, The Physical Chemistry of Lipids, Plenum Press, New York and London, 1986.

[43] A.S. Ulrich, A. Watts, Molecular response of the lipid headgroup to bilayer hydration monitored by 2H-NMR, Biophys. J. 66 (1994) 1441–1449.

[44] A.S. Ulrich, A. Watts, Lipid headgroup hydration studied by 2H-NMR: a link between spectroscopy and thermodynamics, Biophys. Chem. 49 (1994) 39–50.

[45] H.L. Casal, H.H. Mantsch, Polymorphic phase behaviour of phospholipid membranes studied by infrared spectroscopy, Biochim. Biophys. Acta 779 (1984) 381–401.

[46] R.N.A.H. Lewis, R.N. McElhaney, W. Pohle, H. Mantsch, Components of the carbonyl stretching band in the infrared spectra of hydrated 1,2-diacylglycerolipid bilayers: a reevaluation, Biophys. J. 67 (1994) 2367–2375.

[47] B. Bechinger, J.-M. Ruysschaert, E. Goormaghtight, Membrane helix orientation from linear dichroism of infrared attenuated total reflection spectra, Biophys. J. 76 (1999) 552–563.

[48] H. Binder, B. Kohlstrunk, H.H. Heerklotz, Hydration and lyotropic melting of amphiphilic molecules — a thermodynamic study using humidity titration calorimetry, J. Coll. Interface Sci. 220 (1999) 235–249.

[49] G. Klose, B. König, F. Paltauf, Sorption isotherms and swelling of POPC in H_2O and $2H_2O$, Chem. Phys. Lipids 61 (1992) 265–270.

[50] Cevc, G. 1993. In: Water and Biological Macromolecules, ed. E. Westhof, pp. 368–410. Boca Raton: CRC Press

[51] D. Huster, G. Paasche, U. Dietrich et al., Investigation of phospholipid area compression induced by calcium-mediated dextran sulfate interaction, Biophys. J. 77 (1999) 879–887.

[52] R. Kouaouci, J.R. Silvius, I. Graham, M. Pezolet, Calcium-induced lateral phase separations in phosphatidylcholine–phosphatidic acid mixture. A Raman spectroscopic study, Biochemistry 24 (1985) 7132–7140.

[53] H. Binder, U. Dietrich, M. Schalke, H. Pfeiffer, Hydration induced deformation of lipid aggregates before and after polymerization, Langmuir 15 (1999) 4857–4866.

[54] J. Sponer, J.V. Burda, M. Sabat, J. Leszczynski, P. Hobza, Interaction between the guanine–cytosine Watson–Crick DNA base pair and hydrated group IIa (Mg^{2+}, Ca^{2+}, Sr^{2+}, Ba^{2+}) and Group IIb (Zn^{2+}, Cd^{2+}, Hg^{2+}) metal cations, J. Phys. Chem. A 102 (1998) 5951–5957.

[55] C.R. Flach, J.W. Brauner, R. Mendelsohn, Calcium ion interactions with insoluble phospholipid monolayer films at the a/w interface. External reflection–absorption IR studies, Biophys. J. 65 (1993) 1994–2001.

[56] S.F. Martin, G.E. Pitzer, Solution conformation of short-chain phosphatitylcholine substrates of the phosphatidylcholine-preferring PLC of *Bacillus cereus*, Biochim. Biophys. Acta 1464 (2000) 104–112.

[57] D.S. Carr, B.L. Harris, Solutions for maintaining constant relative humidity, Ind. Eng. Chem. 41 (1949) 2014–2015.